Junctionfree Gate Stacked Vertical TFET Hydrogen Sensor at Room Temperature

Sukanya Ghosh, Lintu Rajan, and Arathy Varghese, *Member, IEEE*

Abstract*— Presented through this work is an investigation of junctionfree gate-stacked (SiO_2 + high-k) double gated vertical tunnel field-effect transistor (JF-GS-VTFET) with focus on its hydrogen (H_2) sensing performance at room temperature (RT) for the first time. JF-GS-VTFET with vertically characterized channel length feature minimizes short channel effects (SCEs), elevates gate controllability over regular TFETs without the presence of any sharp doping gradient. A systematical study of the sensing performance is demonstrated through effective variations in Palladium (Pd) and Gold (Au) catalytic metal gate work functions corresponding to the concentration of hydrogen appearing at the gate metal surface. A concentration dependent thorough analysis has been illustrated in terms of energy band, potential, transfer and transient characteristics. Sensing capability of the device have been analyzed in terms of variations in detecting parameters such as transconductance (g_m), off current, on current, threshold voltage and sub-threshold slope in presence of the target gas using SILVACO ATLAS TCAD. At 1.04 ppm H_2 gas concentration, the optimally designed sensor exhibits high I_{ON}/I_{OFF} ratios in the order of ~10^{13} and ~10^{11}, high g_m sensing responses of 99.98% and 98.93%, high off current sensing responses of ~1.895×10^4 and ~1.47×10^4, better sub-threshold swing sensing responses of ~0.71 and ~0.55, increased threshold voltage sensing responses of ~0.27 and ~0.25 for Pd and Au metal gates respectively at RT. Perceptible outcomes in terms of interface trap charge density have also been presented to recognize RT H_2 sensing.

***Index Terms*— Catalytic gate, gate-stack, hydrogen sensor, junctionfree vertical tunnel field-effect transistor (JF-VTFET), sensing response, TCAD.**

I. Introduction

CONTINUOUS shrinkage in device dimensions reduces gate controllability in the channel region with increased leakage current and short channel effects (SCEs) [1], [2]. To reduce such limitations, device architectures with multiple gate terminals such as double gate, FinFETs, gate-all-around FETs, have been proposed [3]. However, the formation of ultra-sharp junction profiles for nanoscale devices at extreme shrinkage of device dimensions becomes complex.

Manuscript submitted for review July 14, 2022. (Corresponding author: lintu@nitc.ac.in).

Sukanya Ghosh and Lintu Rajan are with the Department of Electronics and Communication Engineering, National Institute of Technology, Calicut, Kerala, 673601, India. (e-mail: sukanya_p180068ec@nitc.ac.in; lintu@nitc.ac.in).

Arathy Varghese is with the School of Engineering, Cardiff University, United Kingdom CF24 3AA. (e-mail: VargheseA@cardiff.ac.uk).

Junctionfree (JF) transistor without incorporating any physical junction between source/drain (S/D) and channel, promises great potential in this regard as it is a heavily doped device having identical doping in source, drain and channel regions [4], [5]. In comparison to MOSFETs, TFETs have captured the attention in terms of low leakage current and steeper sub-threshold slope [6]-[8] in continuing Moore's law [9] as well as in overcoming the limitations of FET-based gas sensors [10], [11]. TFET sensors with catalytic metals, polymers, metal and organic compounds-based sensing films [12], [13], device optimization [14]-[16] and device engineering novelty [17], [18] have been explored over recent years. JF-GS-VTFET is a promising nominee as a RT hydrogen sensor involving band-to-band tunneling as integral charge carrier transport mechanism where the work function of the catalytic metal gate shifts in presence of hydrogen. In this regard, Pd and Au are two effective gate metals of preference owing to their excellent catalytic properties and hydrogen solubility for accelerating sensing performance of the device [19], [20]. As a clean energy transporter, the extending demands of hydrogen sensors find its applications in industries, transportation, chemicals, space flights, laboratories, power generation, medicine, petroleum refining, nuclear reactors and so on [21]. This uncolored, odorless and tasteless gas is extremely flammable, has high burning velocity and wide flammable concentration range (4%-75%) which can lead to explosions. Hence early leak detection of hydrogen is the need of the hour. Optical [22], electrochemical [23], acoustic wave variation [24] and calorimetric techniques have already been reported in hydrogen sensing but several drawbacks such as large size, high fabrication cost, slow response, high operating temperature, average sensing response restricts their widespread applications.

To address such issues, for the first time, we focus on the combined advantages of junctionfree, gate-stacking, double gate features and vertical structure to develop a JF-GS-VTFET based RT hydrogen sensor. Scaling limit of gate dielectric such as SiO_2 (<2 nm), imposed by quantum mechanical tunneling, is also responsible for hindering device shrinking. A solution for this problem is to grow a high-k dielectric (HfO_2) on SiO_2, termed as gate-stack [25]. Vertically characterized channel length relaxes the on-chip area without affecting the channel length, thereby reducing the SCEs. High precision sensors demand systematic analysis of the device as well as its sensing performance. Moreover, the effects of work

function variations of catalytic noble metals on energy band, potential, transfer characteristics, threshold voltage, transconductance, transient analysis, on-off current sensing response and sub-threshold slope in presence of air and H_2 have been explored.

II. Device Architecture And Simulation Parameters

The 2-D schematic of the proposed JF-GS-VTFET structure is shown in Fig. 1(a). This junctionfree device consists of highly doped Si body with $1 \times 10^{19}/cm^3$ carrier concentration, Si body thickness t_{Si}= 10 nm to avoid quantum mechanical effects, channel length L= 50 nm and spacer length L_{SP}= 3 nm which defines the gate field closeness to the source side tunneling path. The gate-stack configuration

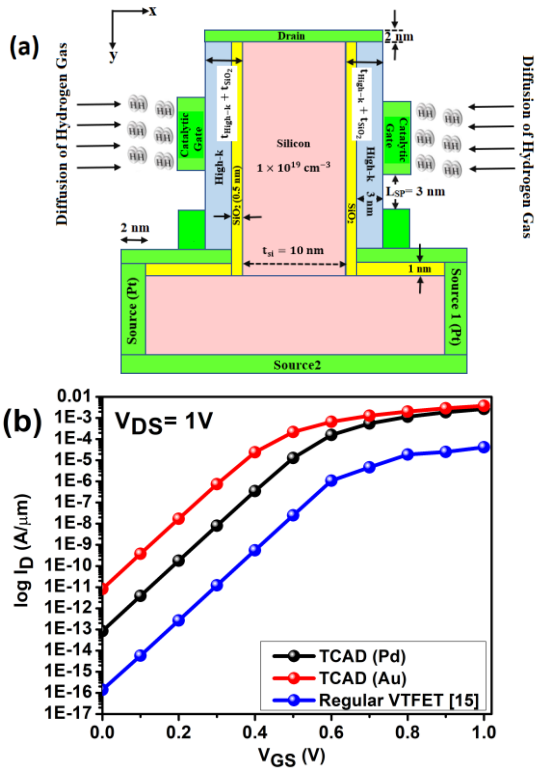

Fig. 1(a). JF-GS-VTFET hydrogen sensor schematic. (b) Calibrated transfer characteristics of JF-GS-VTFET at V_{DS}=V_{GS}= 1V compared with the reported work [15].

includes an oxide thickness t_{OX}= 3.5 nm which is splitted into 3 nm high-k (HfO_2) and 0.5 nm SiO_2 (i.e t_{OX}= $t_{High\text{-}k}$+t_{SiO_2}). P+ pockets have been contrived for source contacts using Platinum (Pt) metal electrodes (work function φ_{ms} = 5.92 eV) on the intrinsic Si substrate. Pd (work function φ_M=5.22 eV) and Au (work function φ_M=5.10 eV) with a thickness of 3 nm have been incorporated as gate metals due to their promising catalytic properties [26]. Random dopant fluctuations (RDFs) can be essentially reduced in the proposed structure as no external doping is required. Structural parameters considered here are optimized to achieve maximum I_{ON}/I_{OFF}. Simulation models [27] invoked are bandgap narrowing (BGN) to consider the effect of high concentration, band to band non-local model (BBT. NONLOCAL) for the impact of tunneling, concentration dependent low field model CONMOB to account for the low field behavior of charge carriers at RT, Lombardi (CVT) mobility model for concentration and field dependent mobility, Shockley– Read– Hall (SRH) recombination model for temperature and doping dependent minority carrier recombination. Fermi-Dirac statistics have been selected to incorporate the variation in properties of a heavily doped region. Calibration of model parameters used in the simulation of JF-GS-VTFET has been performed at V_{DS}=V_{GS}= 1V in accordance with the reported work [15] including the exception of utilizing close proximity of Pt work function as 5.92 eV, gate metals as Pd (work function φ_M=5.22 eV) and Au (work function φ_M=5.10 eV), gate-stack configuration and heavily doped Si body. Calibrated transfer characteristics have been depicted in Fig. 1(b). It can be noticed that drain current values of the proposed structure are higher as compared with regular VTFET structure [15] with promising sub-threshold swing. The possible fabrication steps of the proposed JF-GS-VTFET structure can follow similar steps reported in [28] and is summarized in Fig. 1(c) as:

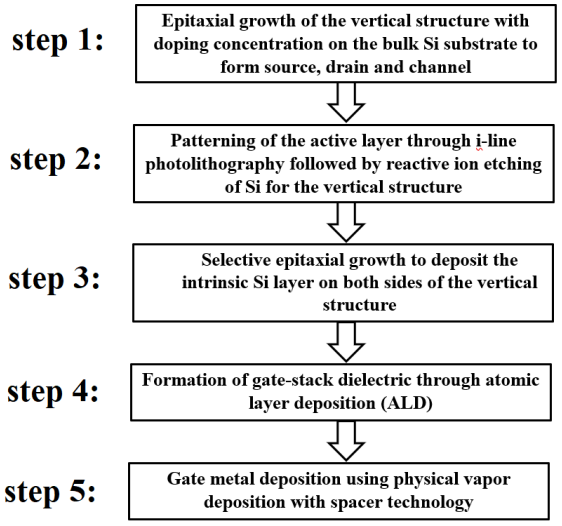

Fig. 1(c). Fabrication steps of JF-GS-VTFET.

III. Hydrogen Sensing Model

As the hydrogen molecules get adsorbed at the surface of the sensing gate, a work function variation of the sensing gate is initiated based upon the interaction between sensing gate metal and hydrogen molecules, thus hydrogen atoms are generated from the dissociation of hydrogen molecules. The effective variation in metal work function ($\Delta\varphi_M$) can be expressed in terms of molar concentration and partial pressure of the target gas [18], [29]:

$$\Delta\varphi_M = M_q - \left[\left(\frac{RT}{4F}\right) * \ln(P)\right] \quad (1)$$

where 'R' is the gas constant = $8.314\ JM^{-1}K^{-1}$, 'T' is the temperature= 300 K and 'F' is Faraday's constant= 96500 CM^{-1} respectively. 'P' is the target gas partial pressure taken as 2.5 Pa [29]. The variations in threshold voltage (V_{TH}) and

flat-band voltage (V_{FB}) owing to the variation in work function ($\Delta\varphi_M$), leads to a change in on and off currents given by equation (2) [18], [30]:

$$V_{FB} = \varphi_M - \varphi_S \pm \Delta\varphi_M \qquad (2)$$

where φ_M and φ_S are the metal and Si work functions respectively. The sub-threshold current can be represented using the expression [30]:

$$I_{Sub-threshold} = I_0 e^{\left(\frac{V_{GS}-V_{TH}}{\eta V_T}\right)}\left[1 - e^{-\frac{V_{DS}}{V_T}}\right] \qquad (3)$$

where V_T is the thermal voltage symbolized as $\frac{KT}{q}$ and $I_0 = \frac{W\mu_0 C_{OX} e^{1.8} V_T^2}{L}$, effective width and length of the transistor are termed as W and L respectively, μ_0 denotes the carrier mobility, η describes the sub-threshold swing factor, C_{OX} is the capacitance of gate oxide/unit area. The shift in off current occurs with the change in sub-threshold current when threshold voltage varies. Equations (1)-(3) present a relationship between the variation in metal work function, threshold voltage and device currents. Under typical environmental conditions, each hydrogen molecule contains two hydrogen atoms. For analyzing sensing behavior of the proposed device, work function-controlled model should be established for which the effective target H_2 concentration can be modeled numerically. Good hydrogen sensing characteristics include extremely low sensing limit (≤1 ppm H_2/air) at RT [31]. In order to study the sensing performance of the device at extremely low H_2 concentration, effective variation in metal work function ($\Delta\varphi_M$) needs to be calculated. Let *x* be the concentration of target hydrogen in ppm which is equivalent to 0.001 *x* gm/l. Dividing it by 2.016 gm/mol (molecular mass of hydrogen) gives the molar concentration equivalent of *x* ppm H_2. Since 1 M comprises of Avogadro number of particles, the surface charge equivalent of *x* ppm H_2:

q_S = Molar concentration (M/l) of *x* ppm H_2 × Avogadro number (4)

where q_S is the surface charge equivalent in coulombs/cm^3 and Avogadro number is 6.023×10^{23}. Now the total interface charge is obtained as:

$$Q = q_H \times q_S \qquad (5)$$

where q_H= charge equivalent/molecule of hydrogen=2 and Q is the total interface charge/cm^3 due to hydrogen. From equation (5), mV equivalent of surface charge evaluates to 0.001Q. Putting the volt equivalent as M_q in equation (1) provides the effective variation in metal work function ($\Delta\varphi_M$) corresponding to *x* ppm H_2 concentration. Thus, the effect of different H_2 concentration on the device characteristics can be realized.

IV. Results And Discussion

Under air exposure, no hydrogen molecules are available for surface adsorption at the sensing gate. Variation in energy band of the proposed structure at the cutline is depicted in Fig. 2(a) and (b) in presence of air and under hydrogen exposure respectively in ON state (V_{DS}=V_{GS}= 1V). The higher work function of Pd as compared to Au results in higher shifting of

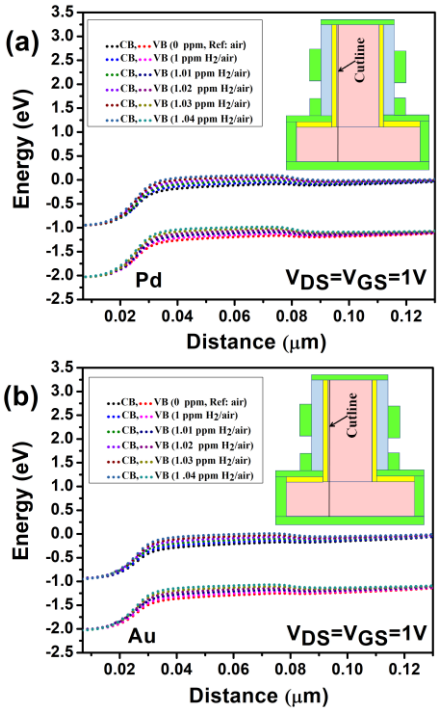

Fig. 2. Variation in energy bands with H_2 concentration in ON state for (a) Pd and (b) Au sensing gates.

the energy band due to the large concentration of p-type charge carriers. Hence with increasing H_2 concentration, energy band shifting becomes higher. Under OFF state, more energy is required for electron tunneling from source valance band to channel conduction band, resulting in higher tunneling barrier. Under ON state, with increasing gate bias energy bands in the channel move in downward direction, valance band in the source gets aligned with conduction band in the channel. This result in significant decrease in tunneling barrier width across the interface between source and channel, hence tunneling current is increased. The positions of energy bands are dependent on the flat band voltage variation which is again dependent on the work function variation of the metal gate under different H_2 concentrations. Fig. 3(a) and (b) exhibits electric field variation with the distance along the channel for different H_2 concentrations in case of Pd and Au sensing gates respectively. It can be observed that the electric field achieves a smaller value in the absence of hydrogen molecules in air whereas it starts increasing with the presence of increasing hydrogen concentrations. Electric field starts increasing steadily at the drain-channel interface with increasing energy, becomes maximum in the channel region, in the spacer-channel interface electric field starts decreasing gradually. At the source-channel interface, minute increments in the electric field peaks are significant due to the reduction in barrier

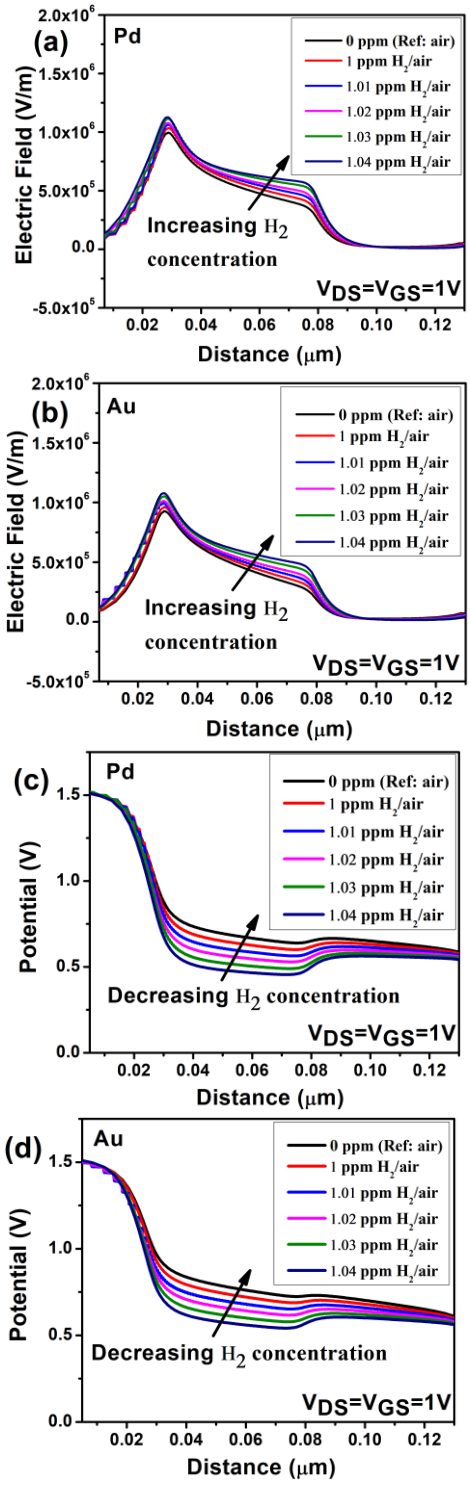

Fig. 3. Variation in (a), (b) electric field and (c), (d) potential profiles for Pd and Au sensing gates with H_2 concentrations under ON state.

width. Eventually, it becomes almost constant owing to linear Fermi level. Potential, being the negative integral of the electric field, decreases with increasing concentration of hydrogen and possesses reverse characteristics than that of the electric field variation [Fig. 3(c) and (d)]. Fig. 4(a)-(b) shows transfer characteristics of the studied device at RT in air and under different H_2 concentrations respectively with the variation of metal gate thickness as inset. As the metal gate thickness increases, surface area to volume ratio increases with increasing recombination rate, leading to a reduction in off current. For the proposed structure, if the metal gate

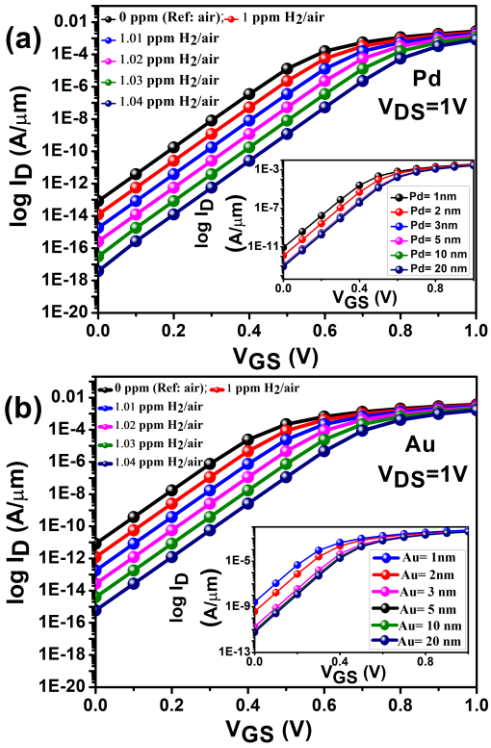

Fig. 4. Transfer characteristics of the studied device in air and under different H_2 concentrations for (a) Pd and (b) Au sensing gates at RT. Insets: Variation of metal gate thickness.

thickness is decreased below 3 nm, off current is observed to be increasing. As the H_2 concentration increases, off current sensing response increases till 3 nm, beyond which off current sensing response reduces. Higher work function of Pd reduces the off current to 10^{-18} A/μm when compared to Au at 1.04 ppm H_2 concentration at RT. On current for Pd is lower than Au. At 1.04 ppm H_2 concentration on current for Pd and Au are 5.02×10^{-5} A/μm and 3.92×10^{-4} A/μm respectively. Effective work function of the metal gate increases with increasing hydrogen concentration and increasing metal gate thickness till 3 nm, beyond which it becomes constant. Under OFF state, more minority charge carriers are induced in the channel with higher metal gate work function. This induces a larger variation in off current than the variation in on current. At the source-channel interface, the energy band diagram becomes less sharp, hence the tunneling probability to the conduction band decreases as the hydrogen concentration increases. Only highly energized electrons are capable to tunnel from channel to drain following band to band tunneling mechanism leading to a reduction in off current with increasing H_2 concentration. Increasing H_2 concentration has significant impact upon off current, hence the sensing response in the sub-threshold region increases, making the studied device more suitable for cost effective low power operations. As the hydrogen molecules interact with the sensing gate, the variation in metal semiconductor work function is considered to be responsible for further band

bending without the presence of Fermi level pinning, resulting in high sensing response in the sub-threshold region [18].

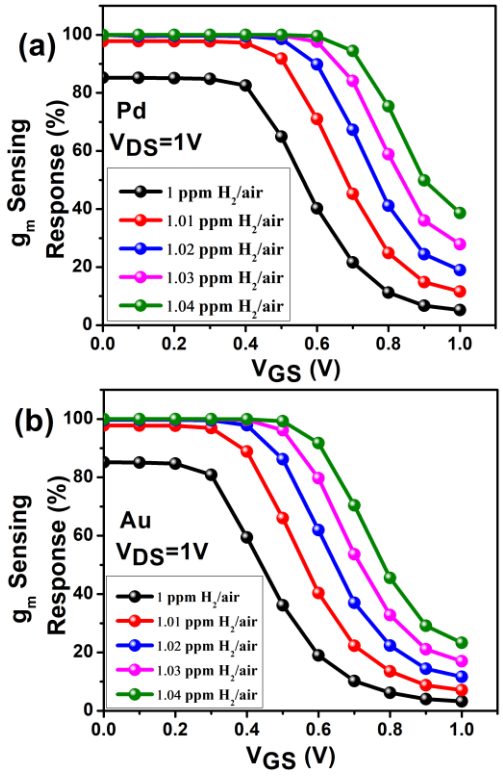

Fig. 5. Transconductance (g_m) sensing response of the studied device in air and under different H_2 concentrations for (a) Pd and (b) Au sensing gates at RT.

Transconductance (g_m) is one of the most crucial parameter of interest to determine device resolution. The transconductance (g_m) sensing response at V_{DS}=1V for different H_2 concentrations with Pd and Au sensing gates have been depicted in Fig. 5(a) and (b) respectively. g_m sensing response starts improving with increasing H_2 concentration. This sensing response can be expressed as $\left|(g_{m(H_2)} - g_{m(air)})/g_{m(air)}\right|$, $g_{m(H_2)}$ and $g_{m(air)}$ are the respective transconductance of the sensor in presence of H_2 and air. The g_m sensing response are observed to be declining with increasing gate voltage. At 1.04 ppm H_2 concentration, the exhibited g_m sensing responses are 99.98% and 98.93% for Pd and Au metal gated devices respectively. Fig. 6(a) and 6(b) illustrates the transient characteristics of the drain current as a function of time for 1 ppm to 1.04 ppm H_2 concentration. Transient variation is observed to increase with H_2 concentration as more hydrogen molecules appear at the catalytic gate metal surface. The drain current returns to its initial baseline value in the absence of H_2, indicating reversible and reusable characteristics of the sensor. For a hydrogen sensor, detecting the variation of target hydrogen molecules on electrical parameters with respect to air is the way to analyze the sensing response. Comparison in hydrogen sensing response of the JF-GS-VTFET for Pd and Au sensing gates with respect to off current has been depicted in Fig. 7(a). Under hydrogen exposure, off current changes with hydrogen concentration. Off current sensing response ($S_{I_{OFF}}$) is defined as the ratio of off current in air to off current in hydrogen i.e $\left|\frac{I_{OFF(air)}}{I_{OFF(H_2)}}\right|$ [18]. In presence of hydrogen, depending upon the

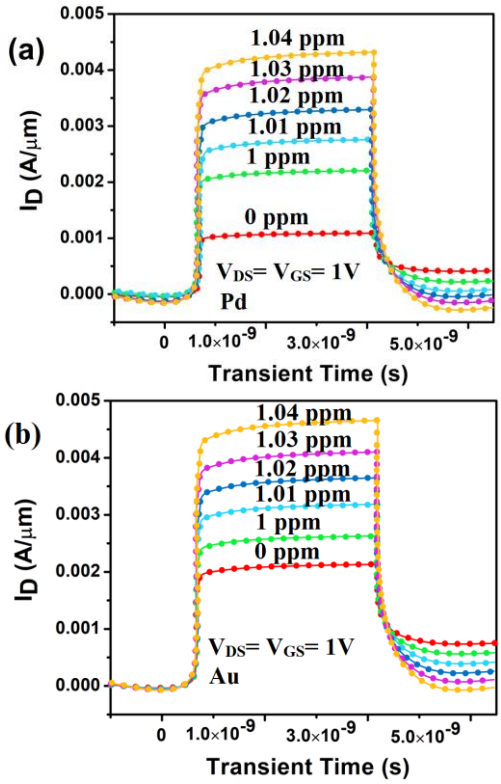

Fig. 6. Transient response analysis of JF-GS-VTFET for (a) Pd and (b) Au sensing gates at RT.

change in gate metal work function the channel gets inverted or depleted without any presence of gate bias, impacting the off current. Higher off current sensing response of the proposed sensor is evident from the transfer characteristics as seen earlier in Fig. 4(a) and (b) respectively compared to its on current sensing response. At 1.04 ppm H_2 concentration and V_{DS}=V_{GS}= 1V, the off current sensing response of the JF-GS-VTFET is observed to be ~1.895×10^4 and ~1.47×10^4 for Pd and Au sensing gates respectively. Based on this significant off current sensing response, it can be noted that the studied device with Pd sensing gate exhibits higher off current sensing response compared to the Au sensing gate as shown in Fig. 7(a). The variation in on current, considered as on current sensing response of Pd and Au for JF-GS-VTFET device with respect to variation in H_2 concentration has been illustrated as inset of Fig. 7(a). On current values were observed to be decreasing with increase in H_2 concentrations. On current sensing response ($S_{I_{ON}}$) is calculated as $\left|(I_{ON(air)} - I_{ON(H_2)})/I_{ON(air)}\right|$, where $I_{ON(air)}$ and $I_{ON(H_2)}$ are the on state drain current when hydrogen molecules are absent and present, respectively at the surface of the sensing gates. The on current sensing response of the JF-GS-VTFET is observed to be 21% and 18% for hydrogen concentration of 1 ppm and 94.9% and 80.4% for hydrogen concentration of 1.04 ppm for Pd and Au sensing gates respectively at RT. Hence due to higher work function and high charge carrier mobility, on current sensing response is more for Pd. It is observed that

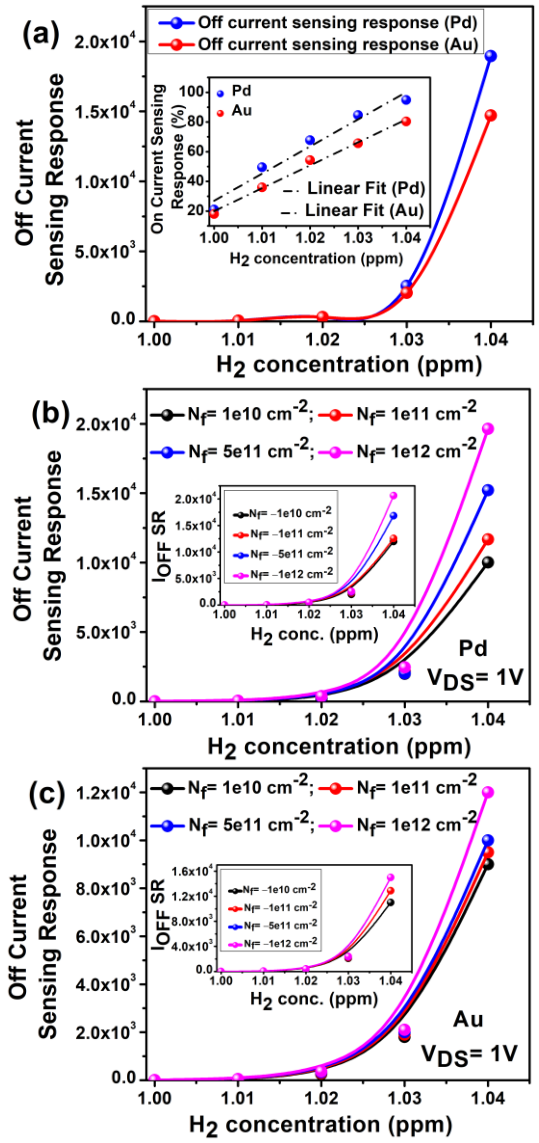

Fig. 7(a) Off current sensing response under different H_2 concentrations for Pd and Au sensing gates at RT. Inset: On current sensing response. (b) Off current sensing response for positive interface trap charges with Pd metal gate. Inset: Off current sensing response for negative interface trap charges. (c) Off current sensing response for positive interface trap charges with Au metal gate. Inset: Off current sensing response for negative interface trap charges.

the on current sensing response is much lower than the off current sensing response. Fig. 7(b) and 7(c) depict the variation in off current sensing response of Pd and Au gate metals as a function of H_2 concentration for different values of positive interface charge densities whereas inset shows off current sensing response for different values of negative interface charge densities. These interface charge densities are selected at the interface between semiconductor and insulator rather than HfO_2/SiO_2 interface as tunneling occurs at the source/channel junction, affecting the device performance. More electron accumulation occurs due to positive interface trap charges compared to zero or negative interface trap charges. Hence the drain current increases with positive interface trap charges whereas it is opposite for negative interface trap charges. The reduction in off current is observed to be more for negative interface trap charges with increasing H_2 concentration, leading to a higher off current sensing response. Fig. 8(a) depicts noticeable threshold voltage shift and their relative threshold voltage as inset with increasing H_2 concentration. The threshold voltage sensitivity (ΔV_{TH}) can be defined as $\left|V_{TH}^{air} - V_{TH}^{H_2}\right|$, where V_{TH}^{air} and $V_{TH}^{H_2}$ are the threshold voltage in air and in H_2 respectively. Threshold voltage is observed to be increasing with increasing H_2 concentration. The higher work function of Pd leads to more rise in threshold voltage as compared to Au. For Pd, an increase in V_{TH} from 0.5 V in air to 0.77 V in 1.04 ppm H_2/air is observed whereas it is 0.38 V in air and 0.63 V in 1.04 ppm H_2/air for Au sensing gate. To explain the sharper characteristics of the

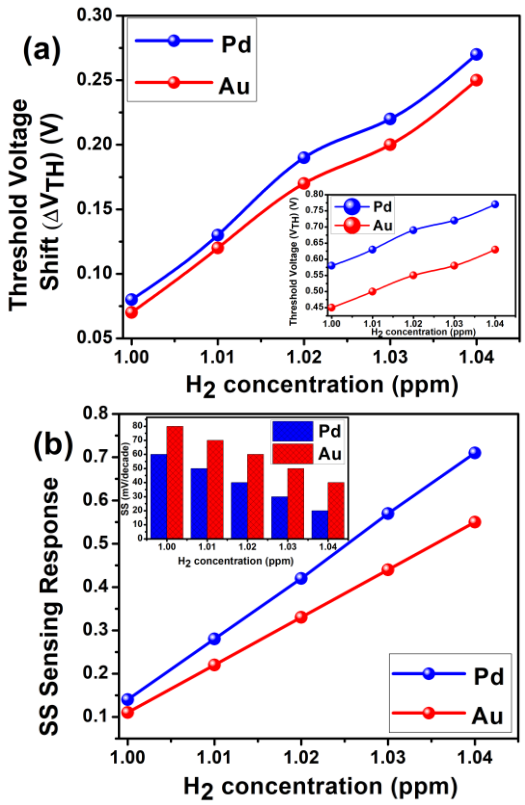

Fig. 8(a) Threshold voltage shift (ΔV_{TH}) of the studied device along H_2 concentration for Pd and Au sensing gates at RT, corresponding threshold voltage plot is depicted as inset. (b) Comparative graphs of SS sensing response of the studied device along H_2 concentration for Pd and Au sensing gates at RT, corresponding SS plot is depicted as inset.

device, sub-threshold swing (SS) is an integral parameter. Its sensing response (S_{SS}) is determined as $\left|\frac{SS^{air}-SS^{H_2}}{SS^{air}}\right|$, where SS^{air} and SS^{H_2} are sub-threshold swing sensing response in air and in H_2 respectively. Fig. 8(b) shows sub-threshold swing sensing response of JF-GS-VTFET for Pd and Au sensing gates respectively along the H_2 concentration and inset shows sub-threshold swing of the corresponding plot along the H_2 concentration. Here it can be observed that the increment in H_2 concentration improves the sub-threshold swing and sub-threshold swing sensing response enhances with increasing H_2 concentration. Pd exhibits better sub-threshold swing sensing response compared to Au. At 1.04 ppm H_2 concentration, SS swing sensing responses with Pd and Au gates are 71% and 55% respectively at RT. RT hydrogen sensing performance

TABLE I
PERFORMANCE COMPARISON AMONG THIS WORK AND THE EXISTING RT HYDROGEN SENSORS

Device Structure	Hydrogen Concentration (ppm)	Sensing Metric	Sensor Response	Ref.
ZnO nanorod decorated with Pd	1000	Current	95%	[32]
Pt Gated AlGaN/GaN MIS HEMT*	1000	Current	1.2×10^3	[33]
Pd/TiO_2/Si MOS*	10000	Conductance	70%	[34]
Pt NP*/TiO_2/GaN Nanowire	1	Current	4%	[35]
Pt/SiO_2/GaN	9970	Current	4.5×10^4	[36]
Pd nanotube	500	Current	1%	[37]
JF-GS-VTFET	1.04	Current	1.895×10^4 (Pd gate) 1.47×10^4 (Au gate)	This Work

*MIS HEMT: Metal Insulator Semiconductor- High Electron Mobility Transistor, NP: Nanoparticle, MOS: Metal Oxide Semiconductor

comparison among the studied device and the existing reports is presented in Table I. In real time scenario, sensing response can get reduced due to undesirable adsorptions, adsorption sites blocking as well as irregular distribution of gas molecules in the target gas mixture. The studied JF-GS-VTFET sensor exhibits excellent hydrogen sensing response even for a 0.01 ppm concentration change. Superior hydrogen sensing responses of 1.895×10^4 and 1.47×10^4 (@ 1.04 ppm H_2/air, RT) have been obtained for Pd and Au sensing gates respectively with low detection limit without any functionalization with graphene. Further device characteristics can be improved through gate engineering and channel optimizations which will ultimately lead to improving sensing performance.

V. Conclusion

In this work, an investigation and a comparative study of the JF-GS-VTFET device with Pd and Au catalytic gates have been presented for the detection of hydrogen gas under RT. Impact of H_2 concentration on various characteristic parameters of the device have been investigated along with their sensing response. Change in off current with H_2 concentration owing to the reaction of hydrogen molecules at the catalytic gate metal surface is incorporated as the integral sensing response parameter as it provides much higher sensing response in comparison to when sensing response is calculated in terms of change in transconductance, on current, threshold voltage shift or SS swing change. Proposed structure with high surface to volume ratio offers better control of gate in channel, resulting in significant change in off current with H_2 concentration with improved sensing response. Off current sensing response with Pd gate provides higher sensing response compared to Au gate. Such devices are promising in the field of ultra-sensitive, low power and cost-effective gas sensing applications.

References

[1] J.-P. Colinge *et al*., "Nanowire transistors without junctions," *Nature Nanotechnol.*, vol. 5, no. 3, pp. 225–229, Feb. 2010.

[2] X. Jin, X. Liu, M. Wu, R. Chuai, J.-H. Lee, and J.-H. Lee, "A unified analytical continuous current model applicable to accumulation mode (junctionless) and inversion mode MOSFETs with symmetric and asymmetric double-gate structures," *Solid-State Electron.*, vol. 79, pp. 206–209, Jan. 2013.

[3] C.-W. Lee, A. Afzalian, N. D. Akhavan, R. Yan, I. Ferain, and J.-P. Colinge, "Junctionless multigate field-effect transistor," *Appl. Phys. Lett.*, vol. 94, no. 5, pp. 053511, Feb. 2009.

[4] C.-W. Lee *et al*., "Performance estimation of junctionless multigate transistors," *Solid-State Electron.*, vol. 54, no. 2, pp. 97–103, Feb. 2010.

[5] C. H. Park *et al.*, "Electrical characteristics of 20-nm junctionless Si nanowire transistors," *Solid-State Electron.*, vol. 73, pp. 7–10, Jul. 2012.

[6] S. Kumar, Y. Singh, B. Singh, and P. K. Tiwari, "Simulation study of dielectric modulated dual channel trench gate TFET-based biosensor," *IEEE Sensors Journal*, vol. 20, no. 21, pp. 12 565–12 573, Jun. 2020.

[7] S. Kumar, B. Singh, and Y. Singh, "Analytical model of dielectric modulated trench double gate junctionless FET for biosensing applications," *IEEE Sensors Journal*, vol. 21, no. 7, pp. 8896–8902, Feb. 2021.

[8] S. Kumar, Y. Singh, and B. Singh, "Extended source double-gate tunnel FET based biosensor with dual sensing capabilities," *Silicon*, vol. 13, no. 6, pp. 1805–1812, Jun. 2021.

[9] G. Wadhwa and B. Raj, "Design, Simulation and performance analysis of JLTFET biosensor for high sensitivity," *IEEE Transactions on Nanotechnology*, vol. 18, pp. 567-574, May. 2019.

[10] S. Han, X. Zhuang, W. Shi, X. Yang, L. Li, and J. Yu, "Poly (3-hexylthiophene)/polystyrene (P3HT/PS) blends based organic field-effect transistor ammonia gas sensor," *Sens. Actuators B Chem.*, vol. 225, pp. 10–15, Mar. 2016.

[11] E. Comini, "Metal oxide nano-crystals for gas sensing," *Anal. Chimica Acta*, vol. 568, pp. 28–40, May 2006.

[12] K. Tsukada, M. Kariya, T. Yamaguchi, T. Kiwa, H. Yamada, T. Maehara,T. Yamamoto, and S. Kunitsugu, "Dual-gate field-effect transistor hydrogen gas sensor with thermal compensation," *Japanese*

Journal of Applied Physics, vol. 49, no. 2R, p. 024206, Feb. 2010.
[13] K. Scharnagl, A. Karthigeyan, M. Burgmair, M. Zimmer, T. Doll, and I. Eisele, "Low temperature hydrogen detection at high concentrations: comparison of platinum and iridium," *Sensors and Actuators B: Chemical*, vol. 80, no. 3, pp. 163–168, Dec. 2001.
[14] G. Wadhwa and B. Raj, "Label free detection of biomolecules using charge-plasma-based gate underlap dielectric modulated junctionless TFET," *Journal of Electronic Materials*, vol. 47, no. 8, pp. 4683–4693, May. 2018.
[15] K. Nigam, P. Kondekar, and D. Sharma, "High frequency performance of dual metal gate vertical tunnel field effect transistor based on work function engineering," *Micro & Nano Letters*, vol. 11, no. 6, pp. 319–322, Jun. 2016.
[16] R. Narang, M. Saxena, M. Gupta et al., "Modeling and simulation investigation of sensitivity of symmetric split gate junctionless FET for biosensing application," *IEEE Sensors Journal*, vol. 17, no. 15, pp. 4853–4861, Jun. 2017.
[17] K. M. Choi and W. Y. Choi, "Work-function variation effects of tunneling field-effect transistors (TFETs)," *IEEE Electron Device Letters*, vol. 34, no. 8, pp. 942–944, Jun. 2013.
[18] R. Gautam, M. Saxena, R. Gupta, and M. Gupta, "Gate-all-around nanowire MOSFET with catalytic metal gate for gas sensing applications," *IEEE Transactions on Nanotechnology*, vol. 12, no. 6, pp. 939–944, Aug. 2013.
[19] S. Ghosh and L. Rajan, "Zinc oxide thin-film transistor with catalytic electrodes for hydrogen sensing at room temperature," *IEEE Transactions on Nanotechnology*, vol. 20, pp. 303-310, Mar. 2021.
[20] S. Ghosh and L. Rajan, "Room temperature hydrogen sensing investigation of zinc oxide Schottky thin-film transistors: Dependence on film thickness," *IEEE Transactions on Electron Devices*, vol. 67, no. 12, pp. 5701-5709, Nov. 2020.
[21] R. Moradi and K. M. Groth, "Hydrogen storage and delivery: Review of the state of the art technologies and risk and reliability analysis," *International Journal of Hydrogen Energy*, vol. 44, no. 23, pp. 12254-12269, May 2019.
[22] J. Hodgkinson and R. P. Tatam, "Optical gas sensing: A review," *Meas. Sci. Technol.*, vol. 24, Nov. 2012, Art. no. 012004.
[23] G. Korotcenkov, S. D. Han, and J. R. Stetter, "Review of electrochemical hydrogen sensors," *Chem. Rev.*, vol. 109, pp. 1402–1433, Feb. 2009.
[24] I. Rýger *et al.*, "GaN/SiC based surface acoustic wave structures for hydrogen sensors with enhanced sensitivity," *Sens. Actuators A Phys.*, vol. 227, pp. 55–62, Feb. 2015.
[25] S. I. Amin and R. K. Sarin, "Enhanced analog performance of dopingless dual material and gate stacked architecture of junctionless transistor with high-k spacer," *Appl. Phys. A, Solids Surf.*, vol. 122, no. 4, pp. 380, Apr. 2016.
[26] S. Ghosh and L. Rajan, "Room Temperature Hydrogen Sensor Using Schottky Contacted Zinc Oxide Thin-Film Transistor: A Comprehensive Investigation," *IEEE Transactions on Electron Devices*, vol. 68, no. 9, pp. 4637-4643, Sept. 2021.
[27] ATLAS Device Simulation Software, Silvaco Int., Santa Clara, CA, USA, 2016.
[28] J. H. Kim, S. Kim, and B.-G. Park, "Double-gate TFET with vertical channel sandwiched by lightly doped Si," *IEEE Transactions on Electron Devices*, vol. 66, no. 4, pp. 1656–1661, Feb. 2019.
[29] A. Varghese, A. Eblabla, and K. Elgaid, "Modeling and simulation of ultrahigh sensitive AlGaN/AlN/GaN HEMT based hydrogen gas detector with low detection limit," *IEEE Sensors Journal*, vol. 21, no. 13, pp. 15361-15368, Apr. 2021.
[30] N. Jayaswal, A. Raman, N. Kumar, and S. Singh, "Design and analysis of electrostatic-charge plasma based dopingless IGZO vertical nanowire FET for ammonia gas sensing," *Superlattices and Microstructures*, vol. 125, pp. 256–270, Jan. 2019.
[31] B. Y Ke and W. C. Liu, "Enhancement of hydrogen sensing performance of a Pd nanoparticle/Pd film/GaOx/GaN-based metal–oxide– semiconductor diode," *IEEE Trans. Electron Devices*, vol. 65, no. 10, pp. 4577–4584, Oct. 2018.
[32] Y. Du, Q. Xue, Z. Zhang, F. Xia, J. Li, and Z. Han, "Hydrogen gas sensing properties of Pd/a-C:Pd/SiO_2/Si structure at room temperature," *Sens. Actuators B, Chem.*, vol. 186, pp. 796–801, Sep. 2013.
[33] J. Ahn, D. Kim, K.-H. Park, G. Yoo, and J. Heo, "Pt-decorated graphene gate AlGaN/GaN MIS-HEMT for ultrahigh sensitive hydrogen gas detection," *IEEE Transactions on Electron Devices*, vol. 68, no. 3, pp. 1255–1261, Feb. 2021.
[34] S. Ratan, C. Kumar, A. Kumar, D. K. Jarwal, A. K. Mishra, and S. Jit, "Fabrication and characterization of titanium dioxide based Pd/TiO_2/Si MOS sensor for hydrogen gas," *IEEE Sensors Journal*, vol. 18, no. 10, pp. 3952–3959, Mar. 2018.
[35] G. S. Aluri, A. Motayed, A. V. Davydov, V. P. Oleshko, K. A. Bertness, N. A. Sanford, and R. V. Mulpuri, "Methanol, ethanol and hydrogen sensing using metal oxide and metal (TiO_2–Pt) composite nanoclusters on GaN nanowires: a new route towards tailoring the selectivity of nanowire/nanocluster chemical sensors," *Nanotechnology*, vol. 23, no. 17, p. 175501, Apr. 2012.
[36] T.-H. Tsai, J.-R. Huang, K.-W. Lin, W.-C. Hsu, H.-I. Chen, and W.-C. Liu, "Improved hydrogen sensing characteristics of a Pt/SiO_2/GaN Schottky diode," *Sens. Actuators B, Chem.*, vol. 129, pp. 292–302, Jan. 2008.
[37] Y. K. Gautam, A. Sanger, A. Kumar, and R. Chandra, "A room temperature hydrogen sensor based on Pd-Mg alloy and multilayers prepared by magnetron sputtering," *Int. J. Hydrogen Energy*, vol. 40, no. 45, pp. 15549–15555, Oct. 2015.

Sukanya Ghosh received her B.Tech degree in Electronics and Communication Engineering from B. P. Poddar Institute of Management and Technology, Kolkata, India and M.Tech degree in VLSI from IEM, Kolkata, India. She is currently working toward the Ph.D. degree in the Department of ECE, National Institute of Technology, Calicut, India. Her research interests include simulation and modeling of semiconductor devices, oxide TFTs, junctionfree TFETs, fabrication and characterization of gas sensors.

Lintu Rajan received the Ph.D. degree in Electronics and Communication Engineering from Malaviya National Institute of Technology, Jaipur, India. She is currently an Assistant Professor with the Department of ECE, National Institute of Technology, Calicut. Her current research interests include fabrication and modeling of semiconductor device-based sensors and MEMS.

Arathy Varghese received B.Tech degree in Electronics and Communication from Kerala University, India, M.Tech degree in VLSI and Embedded system from Mahatma Gandhi University, India, and Ph.D. in Electronics and Communication from the Malaviya National Institute of Technology Jaipur, India. After her doctoral degree, she worked as a postdoctoral researcher at the Indian Institute of Technology Bombay. Currently, she is working as a Research Associate with the School of Engineering, Cardiff University, UK. Her research interests include simulation and modeling of semiconductor devices, and the development of micro and nano electronic devices for high-power, high-frequency, and sensing applications.